Polymorphism of self-assembled colloidal nanostructures of comblike and bottlebrush block copolymers

Inna O Lebedeva, Ekaterina B Zhulina, Oleg V. Borisov

Colloid and Polymer Science
https://doi.org/10.1007/s00396-023-05073-6

ORIGINAL CONTRIBUTION

Polymorphism of self-assembled colloidal nanostructures of comblike and bottlebrush block copolymers

Inna O. Lebedeva[1,2] · Ekaterina B. Zhulina[2] · Oleg V. Borisov[1,2]

Received: 29 November 2022 / Revised: 31 January 2023 / Accepted: 1 February 2023

Abstract
Block copolymers comprising chemically different comblike or bottlebrush blocks can self-assemble in selective solvents giving rise to spherical or wormlike micelles or to polymersomes. The self-consistent field theoretical framework is used for predicting relation between the set of architectural parameters of the blocks (polymerization degrees of the main and side chains, density of grafting of the side chains to the backbone) and structural properties and morphology of the self-assembled aggregates. In particular, it is demonstrated that replacing linear blocks by architecturally symmetrical bottlebrush ones allows tuning the morphology of the self-assembled solution nanostructures.

Keywords Bottlebrush block copolymers · Self-assembly · Colloidal nanostructures · Self-consistent field theory

Introduction

Self-assembly of block copolymers in selective solvents gives rise to diverse nanostructures and represents one of foundations of modern nano- and biomedical technologies [1–5]. Combinations of chemically different blocks with antagonistic properties enable obtaining colloidally stable polymeric nanoparticles with almost unlimited diversity of properties that provides a basis for fabricating smart nanodevices operating in organic or aqueous media and tailored for performing specific functions. Smart nanocontainers for active substances with programmed uptake and release profiles, templates of nanoelectronic devices or nano- and mesoporous hybrid materials, micellar catalysis, colloidal (bio)nanoreactors, etc. are the examples. In the past decades nanosctructures of amphiphilic block copolymers are most actively explored in medicine for anticancer drug and gene delivery purposes [1, 6–8].

Up to now the experimental research focused mostly on exploring and widening the spectrum of chemically different constituent blocks of the copolymers. Only recently it was realized that architectural control over topology of the blocks offers an alternative dimension in the molecular design. That is, replacing linear blocks by regularly branched ones enables fine tuning of the properties of the aggregates without changing chemistry provided that there is reliable control over the blocks architecture.

Furthermore, using branched soluble blocks one can introduce new functionalities which were unattainable for nanoaggregates formed upon self-assembly of linear block copolymers: For example, functionalization of corona hydrophilic blocks with targeted ligands enables exploiting biorecognition mechanisms and thus assuring targeted delivery of drug to specific tissues or cells. In this direction, self-assembly of block copolymers comprising dendritic soluble blocks [9–13] that could substantially increase the number of potentially functionalizable terminal groups exposed to the environment were actively explored. It was demonstrated that complexes of siRNA with nanoassemblies of hydrophobically modified cationic dendrimers were highly efficient in gene therapy [14–16].

While block copolymers with dendritic blocks are synthetically demanding, in many aspects they can be replaced by much more robust comblike and bottlebrush copolymers that possess similar properties (e.g., large number of potentially functionalizable terminal groups in both soluble and insoluble blocks) as dendritic block copolymers. The bottlebrush (co)polymers can be synthesized using one of the elaborated

✉ Oleg V. Borisov
oleg.borisov@univ-pau.fr

[1] Institut des Sciences Analytiques et de Physico-Chimie pour l'Environnement et les Matériaux, UMR 5254 CNRS UPPA, Pau, France

[2] Institute of Macromolecular Compounds of the Russian Academy of Sciences, St. Petersburg, Russia

Published online: 18 March 2023

procedures (grafting to, from, through), which allows controlled variation of the overall molecular mass and degree of branching (grafting density and polymerization degree of side chains) [17]. Furthermore, assembly of triblock copolymers with soluble central bottlebrush block and insoluble (associating) terminal blocks gives rise to "haired mesogels" with unusual (biomimetic) and on demand adjustable through varied molecular architecture mechanical properties [18–20].

Theory of self-assembly of linear diblock copolymers in selective solvents [21–28] was well elaborated in the past decades and enabled one to predict structural properties, including polymorphism of resulting nanoaggregates as a function of the copolymer composition (polymerization degrees of the blocks) and their solubility parameters. As soon as the solubility can be tuned by varying environmental conditions, in particular for ionic and thermosensitive polymers, theory provided also rational basis for encoding stimuli-responsive properties for the block copolymer nanostructures [27].

Recently we have developed a self-consistent field analytical framework in the strong segregation limit for generalizing theory of self-assembly of linear block copolymers to diblock copolymers with regularly, in particular, dendritically branched blocks [29, 30]. The theory predicted how dendronization of one or both (soluble and insoluble) blocks affects structural properties (aggregation number, overall dimensions) and morphology of the nanoaggregates. The developed approach was further extended for predicting properties of spherical micelles formed by comb-shaped or bottlebrush block copolymers, and analysis of so-called bottlebrush to miktoarm transition [31]. The self-consistent field approach was complemented by scaling theory [32] which accounted for effects of local stiffening of the densely grafted bottlebrush blocks.

The goal of the present paper is to go beyond most simple spherical micellar structures and to explore polymorphism of the nanoaggregates formed upon assembly of bottlebrush block copolymers in dilute solutions, that is, to predict how the morphology of the nanostructures can be controlled through tuning polymerization degree of the main and side chains and their grafting densities in the constituent blocks.

The rest of the paper is organized as follows: in "Model and method" we present the model of the bottlebrush block copolymers and outline the self-consistent field formalism. In "Results and discussion" we revise self-consistent theory of spherical micelles formed by bottlebrush block copolymers with the account of finite extensibility of the main chains of the core-forming blocks. Morphological phase diagrams for the nanostructures of the bottlebrush block copolymers are constructed in "Polymorphism of the bottlebrush block copolymer aggregates". The conclusions are summarized in "Conclusions". Detailed description of the employed self-consistent field theoretical approach is presented as Supporting Information.

Model and method

We consider diblock copolymers comprising two chemically different bottlebrush blocks in selective solvent (Fig. 1). Block A has total degree of polymerization (DP) N_A, the DP of the main chain M_A, DPs of side chains n_A and number of monomers in a spacer separating two neighboring grafting points m_A. The set of architectural parameters for the block A will be abbreviated as $\{M_A;n_A;m_A\}$. Block B with total DP N_B is characterized by the corresponding set of parameters $\{M_B;n_B;m_B\}$. Evidently, $n_A = 0$ or $n_B = 0$ correspond to linear respective blocks. The DPs of the blocks are expressed through the sets of architectural parameters as

$$N_{A,B} = M_{A,B}(1 + \frac{n_{A,B}}{m_{A,B}}) \quad (1)$$

Here the main and the side chains of both blocks are assumed to be intrinsically flexible, that is, the monomer unit size a (the same for both blocks) is on the order of the Kuhn segment length. The solvent is assumed to be poor for monomer units of blocks B and moderately good for monomer units of blocks A. The excluded volume parameter for monomer units of the blocks A is $va^3 \cong a^3$.

Self-assembly of such copolymers in dilute solution gives rise to spherical or cylindrical (wormlike) micelles or polymersomes (the latter are thermodynamically equivalent to planar lamellar structures). The condensed cores of the micelles are formed by solvophobic B-blocks

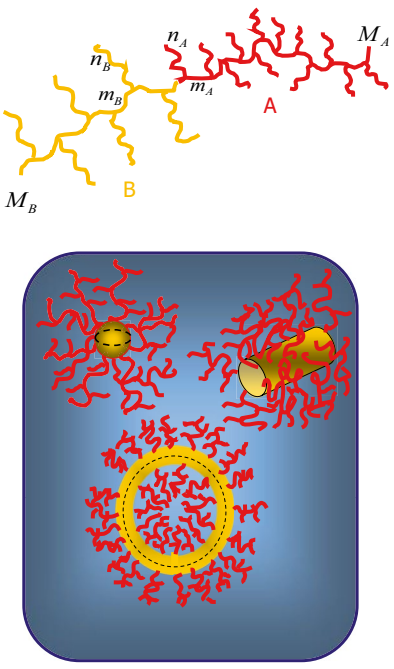

Fig. 1 Bottlebrush block copolymer and diverse solution nanostructures formed in selective solvent good for the block A and poor for the block B

and stabilized by solvated coronae formed by solvophilic blocks *A*. In the following we assume that the core-corona interface is narrow compared to the dimensions of both core and corona domains (strong segregation limit). As a result, the corona domains can be envisioned as swollen brushes formed by blocks *A* tethered to the surface of the core whereas the blocks *B* form a dry brush tethered to inner side of the core-corona interface. Both *A* and *B* blocks are stretched with respect to their unperturbed (swollen or collapsed, respectively) dimensions in the direction perpendicular to the core-corona interface that enables minimizing unfavorable contacts of *B*-monomer units with surrounding solvent.

In order to distinguish block copolymer aggregates of different morphologies we ascribe index $i = 1$ to polymersomes (lamellae), $i = 2$ to cylindrical and $i = 3$ to spherical micelles, respectively. The dense packing of blocks *B* in the core leads to the relation between the core-corona interface area *s* per block copolymer and the size *R* of the core domain (that is, the radius of spherical or cylindrical core or half-thickness of quasi-planar *B*-domain in lamellae)

$$s = \frac{iN_B a^3}{R\phi}, i = 1, 2, 3 \tag{2}$$

where ϕ is the volume fraction of monomer units *B* in the core.

Below we employ the strong-stretching self-consistent field approximation for calculating thermodynamic and structural properties of the corona and core domains. For that we introduce so-called topological ratios η_A, η_B which quantify a relative increase in the conformational free energy penalty for the stretching of *A* and *B* bottlebrush blocks in the corona and core domains, respectively, as compared to the conformational free energy of the respective linear blocks with the same DPs. As demonstrated in ref [33], for bottlebrushes with sufficiently long backbones,

$$\eta_{A,B} \approx (1 + \frac{n_{A,B}}{m_{A,B}})^{1/2} \tag{3}$$

that implies propagation of the elastic stress predominantly through the backbone in the stretched bottlebrush. As follows from Eqs. 1 and 3, the relation between total DP $N_{A,B}$ and the DP of the backbone $M_{A,B}$ for a long molecular brush can be expressed as

$$N_{A,B} \approx M_{A,B}\eta_{A,B}^2 \tag{4}$$

For deriving equilibrium structural properties of the block copolymer aggregates with different morphologies ($i = 1, 2, 3$) we employ procedure of minimization of the free energy (per block copolymer molecule)

$$F^{(i)} = F^{(i)}_{corona} + F^{(i)}_{interface} + F^{(i)}_{core} \tag{5}$$

where the respective terms account for the free energy of the soluble block *A* in the corona, F_{corona}, the free energy of the core-corona interface, $F_{interface}$, and the free energy of the stretched insoluble block *B* in the core, F_{core}. While the term $F^{(i)}_{interface} = \gamma s$ is simply proportional to the area *s* of the core-corona interface per block copolymer ($\gamma k_B T$ being the corresponding surface tension coefficient), the contributions $F^{(i)}_{corona}$ and $F^{(i)}_{core}$ are calculated using previously developed analytical self-consistent field method. The details of these calculations are presented in the Supporting Information.

As demonstrated in refs [26–28], the driving force for morphological transition in block copolymer aggregates is the gain conformational entropy of the core-forming insoluble blocks which is counterbalanced by increasing excluded volume repulsions in the swollen corona domains. The ranges of thermodynamic stability of aggregates with morphologies *i* and $i + 1 (i = 1, 2)$ are separated by binodal lines defined by the condition

$$F^{(i)} = F^{(i+1)} \tag{6}$$

that can be specified as soon as free energies $F^{(i)}$ of the aggregates with different morphologies *i* are known.

Results and discussion

Spherical micelles

Structural properties of spherical starlike, D≫R, and crew-cut R≫D, micelles formed by bottlebrush block copolymers were discussed in details in our previous paper, with the major emphasis on the transition between bottlebrush or miktoarm star conformations of the soluble blocks. Here D is the thickness of the solvated corona formed by A-blocks.

As has been recently predicted by means of scaling arguments [32], because of large volume occupied by insoluble bottlebrush block in the collapsed core domain, the block copolymers with bottlebrush insoluble blocks may form micelles where insoluble blocks are fully stretched. Here we employ mean-field approximation for delineating the ranges of stability and structural properties of the spherical micelles with partially or fully stretched core-forming bottlebrush blocks.

Asymptotic dependences for equilibrium parameters of spherical micelles

The asymptotic power law dependences for equilibrium properties of starlike, $D \gg R$, and crew-cut, $D \ll R$, spherical micelles can be derived by keeping only the dominant terms in the free energy and neglecting the contribution of conformational entropy of the core-forming blocks.

The corona thickness D and the core radius R are given by

$$D/a \cong \begin{cases} \gamma^{3/11}(M_B/\phi_B)^{2/11}M_A^{6/11}v^{1/11}\eta_B^{4/11}\eta_A^{4/11}, & R \ll D \\ \gamma^{1/5}M_A^{4/5}v^{1/5}\eta_A^{4/5}, & R \gg D \end{cases} \tag{7}$$

$$R/a \cong \begin{cases} \gamma^{5/11}(M_B/\phi_B)^{7/11}(v^2M_A)^{-1/11}\eta_B^{14/11}\eta_A^{-8/11}, & R \ll D \\ \gamma^{3/5}(M_B/\phi_B)M_A^{-3/5}v^{-2/5}\eta_B^2\eta_A^{-8/5}, & R \gg D \end{cases} \tag{8}$$

respectively, while the aggregation number $p = (4\pi R^3\phi_B)/(3N_B)$ is given by

$$p \cong \begin{cases} \gamma^{15/11}(M_B/\phi_B)^{10/11}(v^2M_A)^{-3/11}\eta_B^{20/11}\eta_A^{-24/11}, & R \ll D \\ \gamma^{9/5}(M_B/\phi_B)^2v^{-6/5}M_A^{-9/5}\eta_B^4\eta_A^{-24/5}, & R \gg D \end{cases} \tag{9}$$

The boundary between regions of starlike and crew-cut micelles can be derived from the condition $R \cong D$, that is, the micelles become crew-cut at

$$(M_B/\phi_B) \geq \gamma^{-2/5}v^{1/5}M_A^{7/5}\eta_B^{-2}\eta_A^{12/5} \tag{10}$$

As follows from Eq. 8, the starlike micellar core radius, is smaller than the contour length of the main chain of the core-forming B-block, $R \leq M_B$, as long as $M_B \geq M_B^*$, where

$$M_B^* \cong \gamma^{5/4}\phi_B^{-7/4}v^{-1/2}M_A^{-1/4}\eta_B^{7/2}\eta_A^{-2} \tag{11}$$

When $M_B \leq M_B^*$, the core radius reaches the limit of extensibility of the main chain of B-blocks and, upon further decrease in M_B the main chains of the B-blocks remain fully stretched and $R/a \cong M_B$. This imposes new scaling relations for structural properties of the micelles, i.e., for the aggregation number

$$p \cong \frac{M_B^2\phi_B}{\eta_B^2} \tag{12}$$

and for the corona thickness

$$D/a \cong \begin{cases} M_A^{3/5}M_B^{2/5}\phi_B^{1/5}v^{1/5}\eta_B^{-2/5}\eta_A^{4/5}, & R \ll D \\ M_Av^{1/3}\phi_B^{1/3}\eta_B^{-2/3}\eta_A^{4/3}, & R \gg D \end{cases} \tag{13}$$

In Fig. 2 we present a scaling-type diagram of states in (M_A, M_B) coordinates with delineated regimes of thermodynamic stability of spherical starlike and crew-cut micelles which includes also subregimes of micelles with fully stretched main chain in the core-forming blocks. Equations for the boundaries between different regimes and sub-regimes are presented near the lines. At these boundaries smooth crossover for the structural and thermodynamic properties of the micelles in neighboring regions occurs. The regions of stability of the crew-cut micelles merge with the regions of stability of other morphologies marked by shaded areas. At $\eta_A = \eta_B = 1$ the diagram is reduced to that for linear-linear diblock copolymers (marked by dashed lines), whereas an increase in η_A and in η_B beyond unity corresponds to increase in the DPs of the side chains or/and increase in the density of their grafting in the respective blocks. As follows from Eq. 11, at constant M_A and M_B the transition to core-stretched micelles can be triggered by either an increase in η_B or a decrease in η_A.

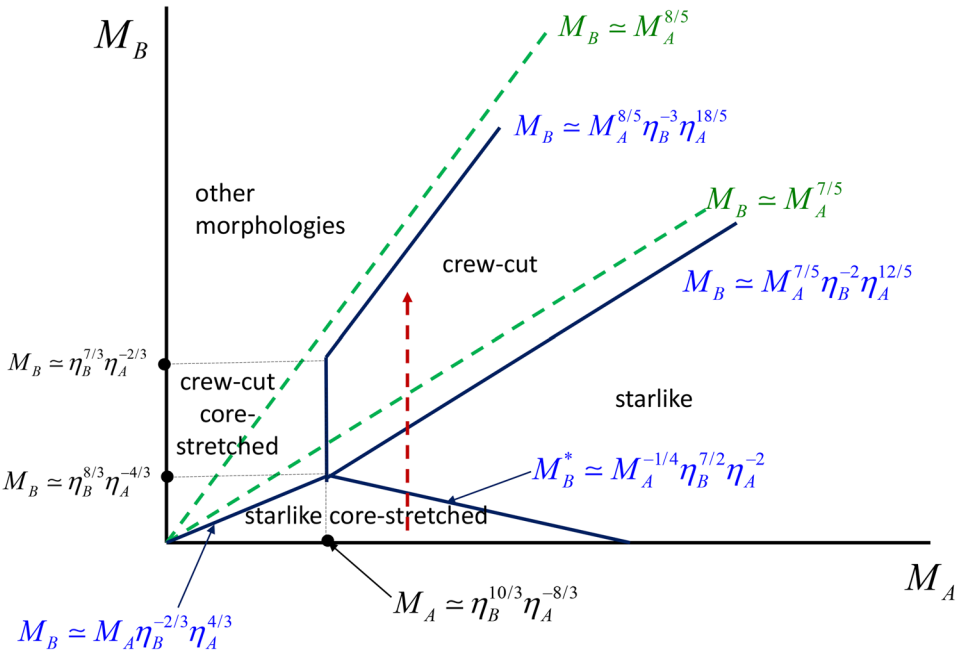

Fig. 2 Schematic diagram of states of spherical micelles formed by diblock copolymers with two bottlebrush blocks in logarithmic M_A, M_B coordinates at $\eta_A^{6/5} \ll \eta_B \ll \eta_A^2$. $\eta_A = (1 + n_A/m_A)^{1/2}$ and $\eta_B = (1 + n_B/m_B)^{1/2}$ are the topological ratios for the respective blocks. Green dashed lines indicate corresponding diagram for micelles of linear-linear ($\eta_A = \eta_B = 1$) diblock copolymers. Equations for boundaries between different regimes are presented near the lines, ϕ, v, γ are set to unity. The cross-section of the diagram by dashed vertical arrow corresponds to variation of M_B at constant M_A in Fig. 3

In Fig. 3a and b we present schematically dependence of micelle core radius R and the aggregation number p on M_B for the cases of $\eta_A = \eta_B = 1$ (linear-linear block copolymer) and for $M_A \geq \gamma \phi_B^{-5/3} \nu^{-2/5} \eta_B^{10/3} \eta_A^{-8/3}$, when an increase in M_B triggers transitions from core-stretched starlike to conventional starlike and further to crew-cut micelles.

Polymorphism of the bottlebrush block copolymer aggregates

While for aggregates of linear block copolymers the morphological transitions from spherical to cylindrical micelles and to polymersomes occur (at constant environmental conditions) when the DPs of the soluble, N_A, and insoluble, N_B, blocks are varied, for bottlebrush block copolymers such transitions can be triggered by changing in the DPs or/and grafting density of the side chains even at constant overall DPs of the blocks. Hence, one can employ topological control over morphology of the block copolymer solution nanostructures.

As one can see from Fig. 4, an increase in the degree of branching of the soluble block A at constant architectural parameters $\{M_B, n_B, m_B\}$ of the insoluble block B leads to extension of the stability range of spherical micelles, shift of the stability range of wormlike micelles to smaller N_A, M_A and shrinkage of the range of stability of polymersomes. This effect is more pronounced if the polymerization degree n_A of the side chains increases at constant polymerization degree M_A of the main chain in the block A (that is, accompanied by at increase in the total polymerization degree N_A of the block A, Fig. 4b). However, the same though weaker trend is observed when moderately

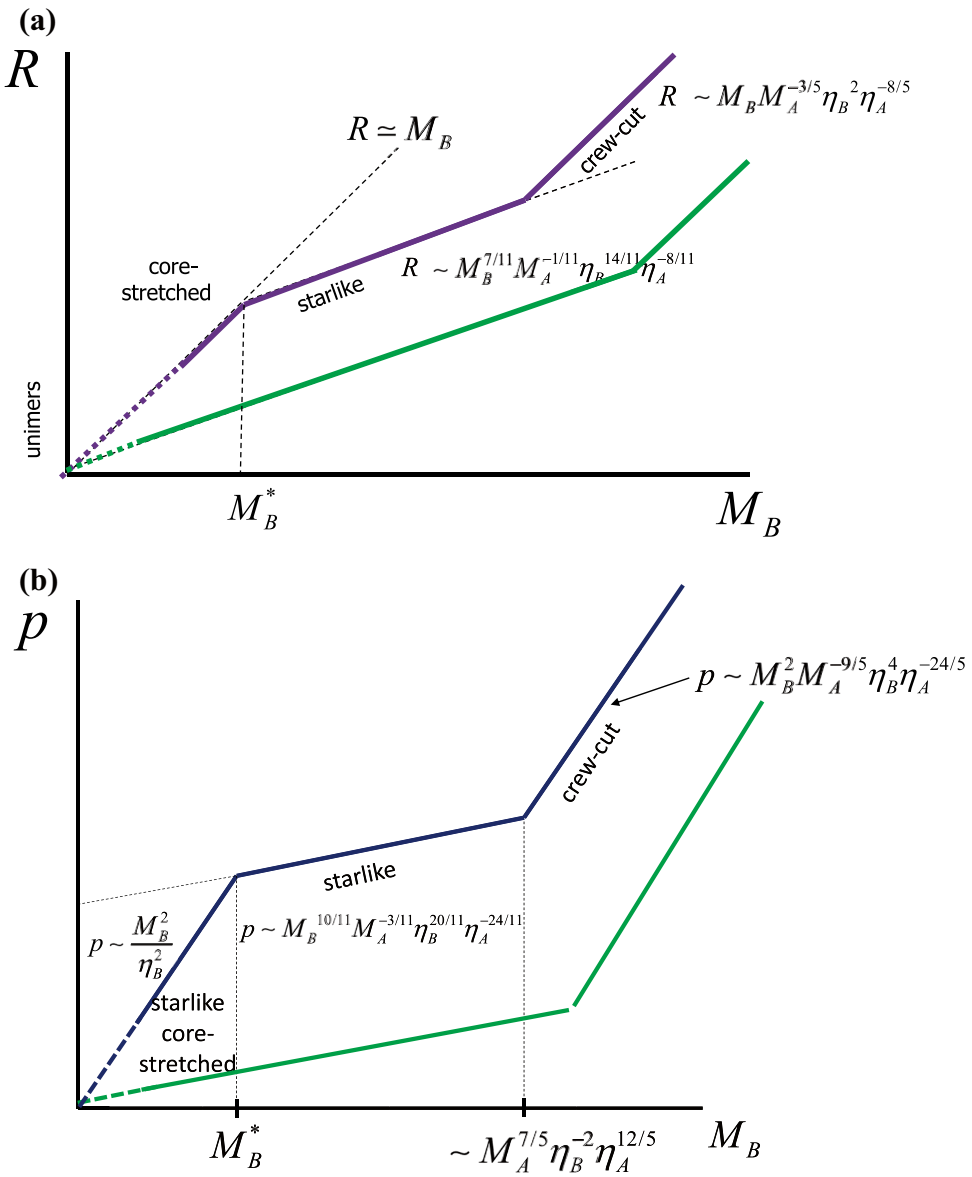

Fig. 3 Schematic dependence of the core radius R (a) and aggregation number p (b) in spherical micelles on M_B in different regimes of the diagram of states, corresponding to cross-section by the red dashed arrow in Fig. 2. Green lines correspond to micelles of linear-linear block copolymers. Asymptotic power law expressions for R and p are presented near the curves

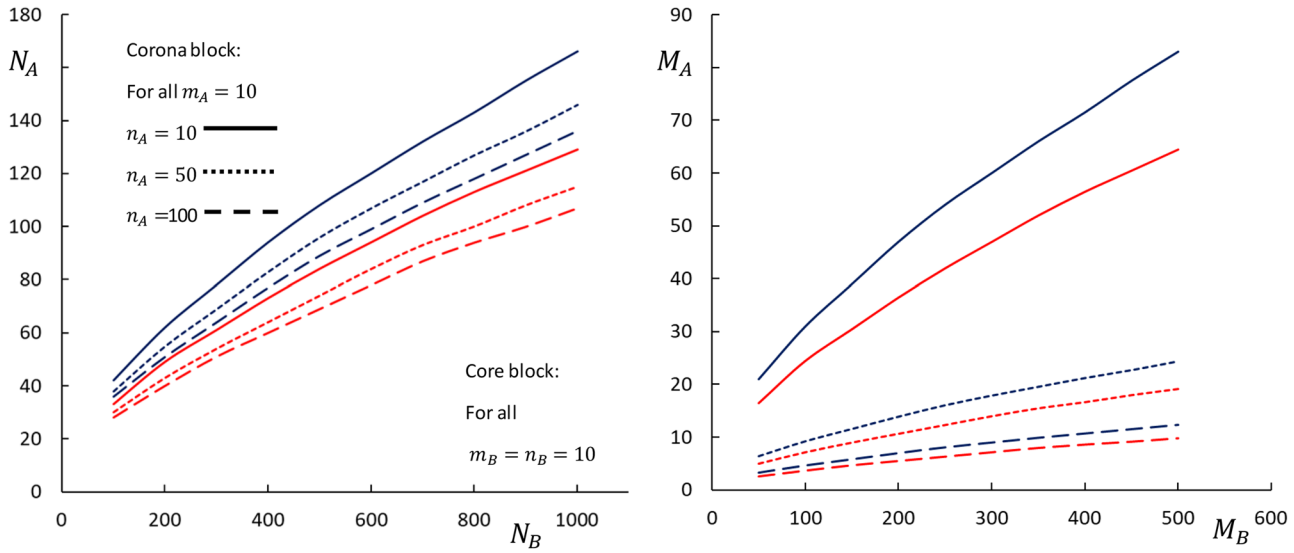

Fig. 4 Morphological diagram of states in (N_A, N_B) (a) and in (M_A, M_B) (b) coordinates at varied polymerization degree n_A of side chains in the soluble block A, as indicated in the figure, and constant architectural parameters $\{n_B = 10, m_B = 10\}$ of the branched insoluble block B. Blue lines denote binodals for spherical-to-wormlike micelles transitions, red lines denote binodals for wormlike micelles-to-polymersomes transitions. Solid lines correspond to linear-linear block copolymers with $n_A/m_A = n_B/m_B = 0$

branched block A is replaced by the stronger branched one with the same total polymerization degree N_A, that is, at increase in the polymerization degree n_A of the side chains leads to a concomitant decrease in M_A and the number P_A of the side chains in the soluble block (Fig. 4a). The extension of the stability range of spherical micelles upon an increase in the branching density n_A/m_A in the soluble bottlebrush block A can be attributed to enhanced excluded volume repulsions between solvated branched blocks as compared to linear (or weakly branched) ones.

The opposite effect on the morphology of the self-assembled structures is caused by an increase in the degree of branching of the insoluble bottlebrush block B at constant parameters $\{M_A, n_A, m_A\}$ of the soluble block A, as demonstrated by Fig. 5: an increase in n_B either at constant N_B or at constant M_B, leads to shrinkage of the stability

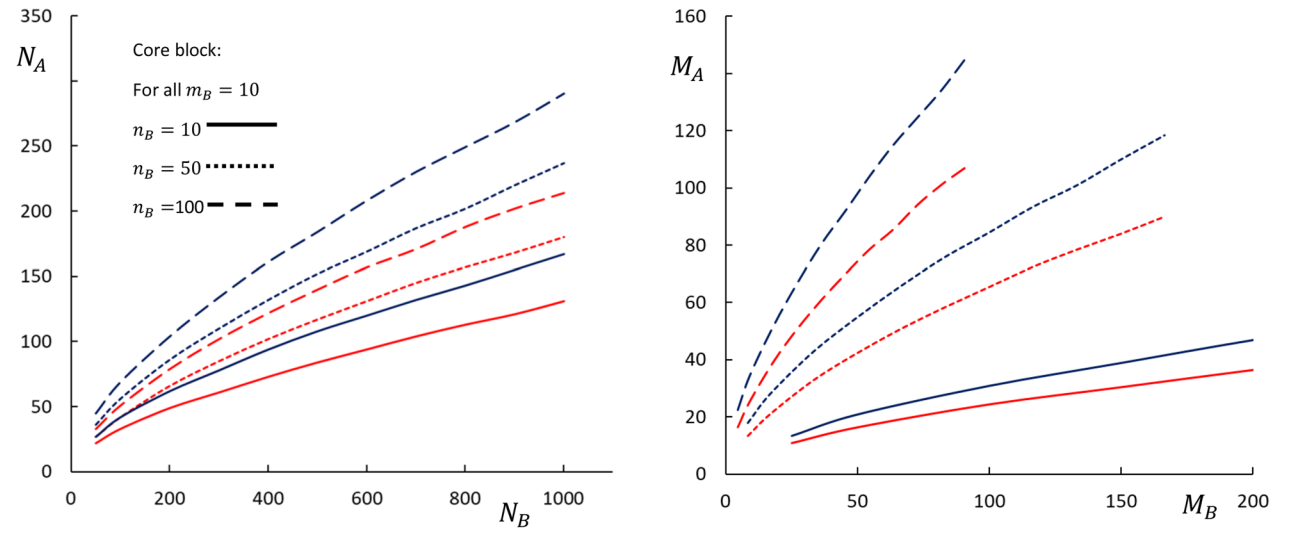

Fig. 5 Morphological diagram of states in (N_A, N_B) (**a**) and in (M_A, M_B) (**b**) coordinates at varied polymerization degree n_B of side chains in the insoluble block B, as indicated in the figure, and constant architectural parameters $\{n_A = 10, m_A = 10\}$ of the branched soluble block A. Blue lines denote binodals for spherical-to-wormlike micelles transitions, red lines denote binodals for wormlike micelles-to-polymersomes transitions. Solid lines correspond to linear-linear block copolymers with $n_A/m_A = n_B/m_B = 0$

range of spherical micelles, extension of the stability range of polymersomes and shift of the stability range of wormlike micelles to larger N_A. These changes in the diagram are explained by an increase in the conformational entropy penalty for stretching of the insoluble B-block upon an increase in n_B at constant M_B due to concomitant increase in the core radius, or due to a decrease in the elastic path length $\sim M_B$ upon an increase in n_B at constant N_B. In the latter case the shift of the boundaries between stability ranges of different morphologies is more pronounced.

In Figs. 6 and 7 we present morphological diagrams of states for bottlebrush block copolymers where branching parameter $n_A/m_A = n_B/m_B \approx \eta_{A,B}^2 - 1$ is the same for both blocks. As a particular case, this corresponds to equal DP of the side chains, $n_A = n_B$ and equal grafting densities in both blocks, $m_A = m_B$.

As one can see in Figs. 6 and 7, an equal increase in n/m in both blocks provokes qualitatively different evolution of the morphology of the nanoaggregates depending on whether total DPs of the blocks, N_A, N_B or DPs of the main chains, M_A, M_B are kept constant. In both cases $\eta_A = \eta_B = 1$ (or $n_A/m_A = n_B/m_B = 0$) corresponds to linear-linear block copolymer, corresponding binodals are plotted in Figs. 6 and 7 by solid lines.

An increase in $n_A/m_A = n_B/m_B$ at constant DPs M_A and M_B of the main chains (Fig. 6) implies growing of the total DPs of the blocks (see Eq. 1) and is accompanied by the shift of the boundaries between morphologies towards smaller M_A and extension of the stability range of spherical micelles on the expence of shrinkage of the stability range of polymersomes. This effect is due to increasing strength of repulsive

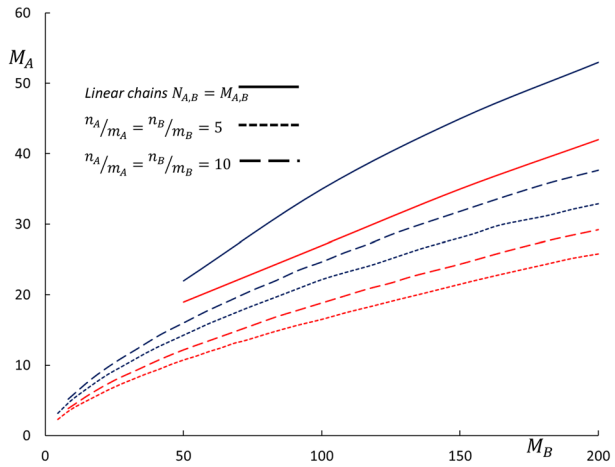

Fig. 6 Morphological diagram of states in (M_A, M_B) coordinates at varied symmetric branching of the both blocks. Blue lines denote binodals for spherical-to-wormlike micelles transitions, red lines denote binodals for wormlike micelles-to-polymersomes transitions. The corresponding values of $n_A/m_A = n_B/m_B$ are indicated near the curves; solid lines correspond to linear-linear block copolymers with $n_A/m_A = n_B/m_B = 0$

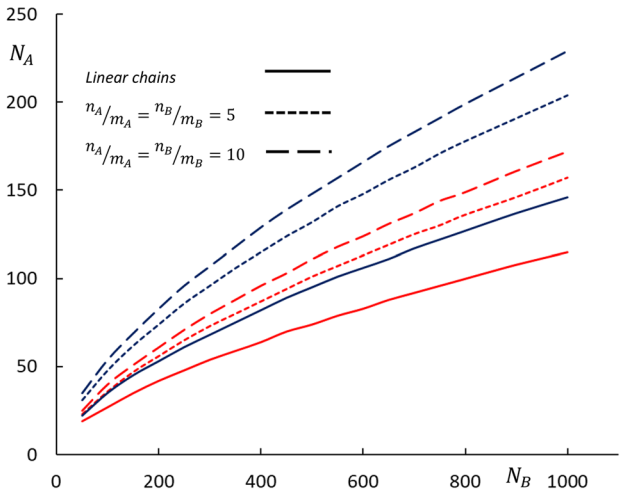

Fig. 7 Morphological diagram of states in (N_A, N_B) coordinates at varied symmetric branching of the both blocks. Blue lines denote binodals for spherical-to-wormlike micelles transitions, red lines denote binodals for wormlike micelles-to-polymersomes transitions. The corresponding values of $n_A/m_A = n_B/m_B$ are indicated near the curves; solid lines correspond to linear-linear block copolymers with $n_A/m_A = n_B/m_B = 0$

interactions between bottlebrush soluble blocks with multiple side chains compared to that for linear ones.

On the contrary, an increase in $n_A/m_A = n_B/m_B$ at constant overall DPs N_A and N_B of the blocks (Fig. 7) implies a simultaneous decrease in the DPs M_A and M_B of the main chains of the blocks and leads to the opposite effect, that is, extension of the stability range of polymersomes and corresponding shrinkage of the range of stability of spherical micelles. This effect is due to increasing entropic penalty for stretching of the main chains of insoluble bottlebrush blocks in the cores of the aggregates.

The presented in Fig. 4, 5, 6, and 7 diagrams were obtained using Eq. 6 and free energies calculated numerically for different morphologies using self-consistent field approximation described in SI and without any pre-assumption concerning ratio R/D between dimensions of the core and the corona domains.

An approximate analytical expression for the binodals can be obtained (as explained in the SI) by assuming $R/D \gg 1$. Since morphological transitions from spherical to wormlike micelles and further to polymersomes are provoked by a concomitant decrease in the entropic penalty for the stretching of the core-forming blocks, for linear block copolymers these transitions occur at $R/D \gg 1$, that is, in the crew-cut domain. Assuming that this is the case for nanoaggregates of the bottlebrush block copolymers and expanding the free energy of the corona in powers of D/R up to linear terms, one arrives to the following approximate expressions for the binodals:

$$N_A^{i\leftrightarrow(i+1)} = [\frac{3}{8}(\frac{3\pi^{2/3}}{5})^{6/5}]^{-5/16}\{i(i+1)[(i+1)^2 b_{i+1} - i^2 b_i]\}^{5/16}.$$

$$N_B^{5/8} v^{-9/16} \frac{\gamma^{3/8}}{\phi^{15/16}} \frac{\eta_B^{5/8}}{\eta_A^{1/4}} \tag{14}$$

or, equivalently,

$$M_A^{i\leftrightarrow(i+1)} = [\frac{3}{8}(\frac{3\pi^{2/3}}{5})^{6/5}]^{-5/16}\{i(i+1)[(i+1)^2 b_{i+1} - i^2 b_i]\}^{5/16}.$$

$$M_B^{5/8} v^{-9/16} \frac{\gamma^{3/8}}{\phi^{15/16}} \frac{\eta_B^{15/8}}{\eta_A^{9/4}} \tag{15}$$

For the analysis of the effect of variation of the side chains lengths and grafting densities in both blocks, it is convenient to present Eqs. 14 and 15 as

$$N_A^{i\leftrightarrow(i+1)} = Q_i N_B^{5/8} \eta_B^{5/8} \eta_A^{-1/4} \tag{16}$$

or

$$M_A^{i\leftrightarrow(i+1)} = Q_i M_B^{5/8} \eta_B^{15/8} \eta_A^{-9/4} \tag{17}$$

where

$$Q_i = [\frac{3}{8}(\frac{3\pi^{2/3}}{5})^{6/5}]^{-5/16}\{i(i+1)[(i+1)^2 b_{i+1} - i^2 b_i]\}^{5/16} v^{-9/16} \frac{\gamma^{3/8}}{\phi^{15/16}} \tag{18}$$

is a prefactor independent of architectural parameters $M_{A,B}$ and $\eta_{A,B}$ of the blocks, and notably $Q_2 \geq Q_1$.

By setting $\eta_A = \eta_B = (1 + n/m)^{1/2}$ one confirms the trends in evolution of the binodals upon an increase in n/m depicted in Figs. 6 and 7.

Evidently, asymmetric branching, that is, grafting of side chains with different DPs and with different grafting densities to the soluble and insoluble blocks also enables tuning of the morphology of the bottlebrush block copolymer aggregates: An increase in (n_A/m_A) at constant (n_B/m_B) results in polymersome-wormlike-spherical micelle transition, while an increase in (n_B/m_B) at constant (n_A/m_A) leads to the opposite sequence of morphological transitions.

Conclusions

Morphology of the solution nanostructures formed by bottlebrush block copolymers in selective solvents can be tuned through controlled variation of the DPs of side chains and grafting density. Increasing branching parameter (n_A/m_A) of the soluble blocks provokes stabilization of spherical micelles, whereas increasing branching parameter (n_B/m_B) of the insoluble blocks leads to the opposite effect.

Introducing symmetric branching of both blocks $(n_A/m_A = n_B/m_B)$ leads to extension of range of stability of polymersomes and shrinkage of the stability range of spherical micelles as compared to linear block copolymers with the same DPs of both blocks. However, if the DPs of the main chains of the blocks are kept constant and grafting density or/and DP of the side chains increase, the effect is the opposite: the spherical micelles are stabilized and the stability range of polymersomes shrinks. Remarkably, as it was demonstrated in ref [38], symmetric branching of strongly incompatible blocks does not alter the morphology of microphase segregated superstructures in solvent-free melts of copolymers with comblike or bottlebrush blocks compared to the superstructures formed by linear block copolymers with similar DPs of the blocks.

We have also explored in detail novel features in spherical micelles formed by bottlebrush block copolymers: Starlike micelles with fully stretched core blocks are described. These micelles are characterized by the exponents of the power law dependences which differ from those for micelles formed by linear block copolymers or bottlebrush block copolymers with partially stretched main chains of the insoluble blocks. Because of extra volume occupied by side chains of the insoluble block, the core radius (which depends only on the overall DP of the insoluble block) is systematically larger than the core radius in the micelle formed by copolymer with linear insoluble block with the same DP as that of the main chain in the bottlebrush block. As a result, the main chain of the insoluble bottlebrush block reaches the limit of extensibility under the same conditions when a linear insoluble block (without side chains) is still stretched below its contour length.

Glossary

a	monomer unit length
D	thickness of the swollen corona formed by blocks A
F	Helmholtz free energy
$M_{A,B}$	polymerization degrees of the main chains in A and B blocks
$n_{A,B}$	polymerization degrees of side chains in A and B blocks
$m_{A,B}$	polymerization degrees of spacers in A and B blocks
N_A, N_B	total degrees of polymerization of blocks A and B, respectively
p	aggregation number in a spherical micelle
R	radius of the condensed core formed by insoluble blocks B
s	surface area of the micellar core per block copolymer
va^3	excluded volume of a monomer unit in block A
$\gamma k_B T$	surface tension coefficient on the core-corona interface
ϕ_B	volume fraction of monomer units of the B-block in the core
$\eta_{A,B}$	topological ratios in A and B blocks

Funding This work was financially supported by Ministry of Research and Education of the Russian Federation within State Contract N 14.W03.31.0022, by the ANR-DFG TOPOL Project ANR-20-CE92-0044, by the European Union's Horizon 2020 research and innovation program under the Marie Sklodowska-Curie grant agreement no. 823883.

Declarations

Conflict of interest The authors declare no competing interests

References

1. Lazzari M, Lin G, Lecommandoux S (2006) Block copolymers in nanoscience. Wiley-VCH, Weinheim
2. Mai Y, Eisenberg E (2012) Self assembly of block copolymers. Chem Soc Rev 41:5969–5985
3. Schacher FH, Rupar PA, Manners I (2012) Functional block copolymers: nanostructured materials with emerging applications. Angew Chem Int Ed 41:5969–5985
4. Gröschel AH, Müller AHE (2015) Self-assembly concept for multicompartment nanostructures. Nanoscale 7:11841–11876
5. Tritschler U, Pearce S, Gwyther J, Whittell GR, Manners I (2017) 50th anniversary perspective: Functional nanoparticles from the solution self-assembly of block copolymers. Macromolecules *50*, 3439-3463
6. Nishiyama N, Kataoka K (2006) Nanostructured devices based on block copolymer assemblies for drug delivery: designing structures for enhanced drug function. Adv Polym Sci 193:67–101
7. Miyata K, Nishiyama N, Kataoka K (2012) Rational design of smart supramolecular assemblies for gene delivery: Chemical challenges in the creation of artificial viruses. Chem Soc Rev 41:2562–2574
8. Sakai-Kato K, Nishiyama N, Kozaki M et al (2015) General considerations regarding the in vitro and in vivo properties of block copolymer micelle products and their evaluation. J Control Release 210:76–83
9. Wurm F, Frey H (2011) Linear-dendritic block copolymers: the state of the art and exciting perspectives. Progress in Polymer Science 36:1–52
10. Blasco E, Pinol M, Oriol L (2014) Responsive linear-dendritic block copolymers. Macromolecular Rapid Communications 35(12):1090–1115
11. Garcia-Juan H, Nogales A, Blasco E, Martinez JC, Sics I, Ezquerra TA, Pinol M, Oriol L (2016) Self-assembly of thermo and light responsive amphiphilic linear dendritic block copolymers. European Polymer Journal 81:621–633
12. Mirsharghi S, Knudsen KD, Bagherifam S, Niström B, Boas U (2016) Preparation and self-assembly of amphiphilic polylysine dendrons New. J Chem 40:3597–3611
13. Fan X, Zhao Y, Xu W, Li L (2016) Linear-Dendritic Block Copolymer for Drug and Gene Delivery. Mater Sci Eng C 62:943–959
14. Yu T, Liu X, Bolcato-Bellemin AL, Wang Y, Liu C, Erbacher P, Qu F, Rocchi P, Behr JP, Peng L (2012) An amphiphilic dendrimer for effective delivery of small interfering RNA and gene silencing in vitro and in vivo. *Angew.Chem., Int.Ed.* 51, 8606-8612
15. Liu X, Zhou J, Yu T, Chen C, Cheng Q, Sengupta K, Huang Y, Li H, Liu C, Wang Y, Pososso P, Wang M, Cui Q, Giorgio S, Fermeglia M, Qu F, Pricl S, Shi Y, Liang Z, Rocchi P, Rossi JJ, Peng L (2014) Adaptive Amphiphilic Dendrimer-Based Nanoassemblies as Robust and Versatile siRNA Delivery Systems. Angew. Chem., Int.Ed. 126, 12016-12021
16. Liu X, Liu C, Zhou J, Chen C, Qu F, Rossi JJ, Rocchi P, Peng L (2015) Promoting siRNA delivery via enhanced cellular uptake using an arginine-decorated amphiphilic dendrimer. Nanoscale 7:3867–3875
17. Yuan J, Müller AHE, Matyjaszewski K, Sheiko S (2012) In *Polymer Science: A Comprehensive Reference*; Matyjaszewski, K., Möller, M., Eds.-in-Chief; Elsevier, Amsterdam.
18. Zhang D, Dashtimoghadam E, Fahimipour F, Hu X, Li Q, Bersenev EA, Ivanov DA, Vatankhah-Varnoosfaderani M, Sheiko SS (2020) Tissue-adaptive materials with independently regulated modulus and transition temperature. Adv Mater 32:2005314
19. Vashahi F, Martinez MR, Dashtimoghadam E, Fahimipour F, Keith AN, Bersenev EA, Ivanov DA, Zhulina EB, Popryadukhin P, Matyjaszewski K, Vatankhah-Varnosfaderani M, Sheiko SS (2022) Injectable bottlebrush hydrogels with tissue-mimetic mechanical properties. Sci Adv 8, eabm2469
20. Li T, Huang F, Diaz-Dussan D, Zhao J, Srinivas S, Narain R, Tian W, Hao X (2020) Preparation and Characterization of Thermoresponsive PEG-Based Injectable Hydrogels and Their Application for 3D Cell Culture. Biomacromolecules 21:1254–1263
21. de Gennes PJ (1978) Macromolecules and Liquid Crystals: Reflections on Certain Lines of Research. in *Solid State Physics*, Academic Press, NewYork, p. 1-17
22. Halperin A (1987) Polymeric micelles: A star model. Macromolecules 20:2943–2946
23. Halperin A, Alexander S (1989) Polymeric micelles: their relaxation kinetics. Macromolecules 22:2403–2412
24. Zhulina YB, Birshtein TM (1985) Conformations of block copolymer molecules in selective solvents (micellar structures) Polym. Sci USSR 27:570–578
25. Birshtein TM, Zhulina EB (1989) Scaling theory of supermolecular structures in block copolymer solvent systems: 1. Model of micellar structures. Polymer 30:170–177
26. Zhulina EB, Adam M, Sheiko S, LaRue I, Rubinstein M (2005) Diblock copolymer micelles in a dilute solution. Macromolecules 38:5330
27. Borisov OV, Zhulina EB, Leermakers FAM, Müller AHE (2011) Self-assembled structures of amphiphilic ionic block copolymers: theory, self-consistent field modelling and experiment. Adv Polym Sci 241:57–129
28. Zhulina EB, Borisov OV (2012) Theory of block copolymer micelles: recent advances and current challenges. Macromolecules 45:4229–4240
29. Lebedeva IO, Zhulina EB, Borisov OV (2018) Theory of Linear-Dendritic Block Copolymer Micelles. ACS Macro Letters 7:811–816
30. Lebedeva IO, Zhulina EB, Borisov OV (2019) Self-assembly of linear-dendritic and double-dendritic block copolymers: from spherical micelles to dendrimersomes. Macromolecules 52(10):3655–3667
31. Lebedeva IO, Zhulina EB, Borisov OV (2021) Self-assembly of Bottlebrush Block Copolymers in Selective Solvent: Micellar Structures. Polymers 13:1351
32. Zhulina EB, Borisov OV (2021) Micelles Formed by AB Copolymer with Bottlebrush Blocks. Scaling Theory J Phys Chem B 125(45):12603–12616
33. Mikhailov IV, Zhulina EB, Borisov OV (2020) Brushes and lamellar mesophases of comb-shaped (co)polymers: a self-consistent field theory. Physical Chemistry Chemical Physics 22:23385–23398
34. Pickett GT (2001) Classical Path Analysis of end-Grafted Dendrimers: Dendrimer Forest. Macromolecules 34:8784–8791
35. Zook TC, Pickett GT (2003) Hollow-Core Dendrimers Revised. Physical Review Letters 90(1)
36. Zhulina EB, Leermakers FAM, Borisov OV (2015) Ideal mixing in multicomponent brushes of branched macromolecules. Macromolecules 48(23):5614–5622
37. Semenov AN (1985) Contribution to the theory of microphase layering in block-copolymer melts. Sov Phys JETP 61:733–742

38. Zhulina EB, Sheiko SS, Dobrynin AV, Borisov OV (2020) Microphase segregation in the melts of bottlebrush block copolymers. Macromolecules 53(7):2582–2593